J. Membrane Biol. 110, 29–38 (1989)

The Journal of
Membrane Biology

Activation Kinetics of Single High-Threshold Calcium Channels in the Membrane of Sensory Neurons from Mouse Embryos

P.G. Kostyuk†, Ya. M. Shuba†, and V.I. Teslenko†
†A.A. Bogomoletz Institute of Physiology, Kiev, USSR, and ‡Institute for Theoretical Physics, Kiev, USSR

Summary. Activation kinetics of single high-threshold inactivating (HTI or *N*-type) calcium channels of cultured dorsal root ganglion cells from mouse embryos was studied using a patch-clamp method. Calcium channels displayed bursting activity. The open-time histogram was single exponential with an almost potential-independent mean open time τ_{op} = 1.2 msec. The closed-time histogram was multicomponent; at least three of the components were associated with the activation process. The "fast" exponential component with the potential-independent time constant τ^f_{cl} = 0.9 msec included all intraburst gaps, while two "slower" ones with potential-dependent time constants τ^s_{cl} and τ^{us}_{cl} described shut times between bursts and between clusters of bursts. The burst length histogram was biexponential. The "fast" component with a relatively potential-independent time constant τ^f_{bur} = 0.6 msec described short, isolated channel openings while the "slow" component characterized real bursts with a potential-dependent mean life time. The waiting-time histogram could be fitted by a difference of two exponentials with time constants being the same as τ^s_{cl} and τ^{us}_{cl}. The data obtained were described in the frame of a 4-state sequential model of calcium channel activation, in which the first two stages are formally attributed to potential-dependent transmembrane transfer of two charged gating particles accompanying the channel transitions between three closed states, and the third one to fast conformational changes in channel protein leading to the opening of the channel. The rate constants for all transitions were defined. The validity of the proposed model for both low-threshold inactivating (LTI or *T*-type) and high-threshold noninactivating (HTN or *L*-type) calcium channels is discussed.

Key Words single calcium channels · activation kinetics · 4-state model

Introduction

As is known from our early experiments with intracellular perfusion, the activation of calcium currents in snail and mammalian neurons can be well described by a modified Hodgkin-Huxley model using a square power of the *m*-variable (Kostyuk, Krishtal & Shakhovalov, 1977; Fedulova, Kostyuk & Veselovsky, 1981). These data have been confirmed in other laboratories (Byerly & Hagiwara, 1982; Byerly, Chase & Stimers, 1984). The model suggests the presence of two independent equally charged gating particles, whose transition along the channel axis can be described by first order kinetic equations with potential-dependent rate constants. This model fits well to the data about stationary characteristics and kinetics of asymmetric displacement currents accompanying the activation of calcium channels, which may represent the movement of the suggested gating particles (Kostyuk, Krishtal & Pidoplichko, 1981). However, spectrum analysis of calcium current fluctuations and direct analysis of single calcium channel activity have shown the insufficiency of the proposed model. The data obtained led to the assumption about the presence of a fast potential-independent kinetic stage that precedes the open state of the channel (Krishtal, Pidoplichko & Shakhovalov, 1980; Fenwick, Marty & Neher, 1982; Brown, Tsuda & Wilson, 1983; Hagiwara & Byerly, 1983; Hagiwara & Ohmori, 1983; Brown, Lux & Wilson, 1984; Shuba & Savchenko, 1985). Both approaches to the understanding of kinetic mechanisms of calcium channels are little related to each other. Therefore, in the present paper, we made a detailed analysis of the activity of single high-threshold inactivating (HTI) calcium channels on a very convenient object (cultured neurons from dorsal root ganglia of mouse embryos) using a 4-state model of their gating mechanisms

$$R \underset{\beta}{\overset{2\alpha}{\rightleftharpoons}} C \underset{2\beta}{\overset{\alpha}{\rightleftharpoons}} A \underset{b}{\overset{a}{\rightleftharpoons}} O \qquad (1)$$

which is a natural generalization of both approaches. In this model α and β represent potential-dependent rate constants for the transitions from resting state R into intermediate closed C and activated A states; a and b are those for transitions between activated A and open O states. *A priori* one would expect four independent rate constants be-

tween R, C and A states in Eq. (1). Fortunately, in the spirit of the modified Hodgkin-Huxley model, the one proposed maintains some physical symmetry and simplicity while still adequately describing many of the phenomena observed during the analysis of the calcium channel gating.

A theoretical description of the main stochastic properties of the proposed simplified model is given in the Appendix.

Materials and Methods

The main part of experiments was performed on cultured dorsal root ganglion (DRG) neurons from 12–14 day-old mouse embryos using a patch-clamp technique in its cell-attached configuration (Hamill et al., 1981). The procedure for cell cultivation was described in detail by Skibo and Koval (1984). Most cells were taken after 5 days in culture for kinetic characterization of HTI calcium channels. Neuroblastoma cells of clone NIF-115 and PC-12 pheochromocytoma cells were used to check the validity of the proposed kinetic model for low-threshold inactivating (LTI) and high-threshold noninactivating (HTN) calcium channels. These cells were cultured as described elsewhere (Amano, Richardson & Nirenberg, 1972; Green & Tischler, 1976).

To avoid uncertainties in the cell resting potential (V_r) during single-channel recording in the cell-attached configuration, it was zeroed by placing the cells into an extracellular solution containing a high concentration of K^+ (mM): 140 K-aspartate, 10 K-EGTA, 20 HEPES, 5 $MgCl_2$, pH 7.3. Some experiments on cultured DRG neurons were, however, carried out on cell cultures placed in normal Ringer solution (mM): 120 NaCl, 4 KCl, 5 $CaCl_2$, 2 $MgCl_2$, 10 glucose, 10 HEPES, pH 7.3. In this case V_r, which according to direct microelectrode measurements and indirect estimations was near −15 mV, was taken into consideration. This low value of resting potential can be explained by the relatively young age of the growth culture when the essential part of the cell population is in the stage of bipolar neuroblasts (*see* e.g., Tchuppina, 1981). The low value of V_r for investigated cells does not preclude their use in the experiments reported here, though according to our observations they are not yet able to produce full-sized action potentials.

During single Ca channel recording, 60 mM Ca^{2+} were present in the pipette solution as a permeant cation through Ca channel. 2 mM $MgCl_2$, 40 mM TEA-Cl, 10 mM HEPES and 10^{-6} M TTX were also added, and pH was titrated to 7.3 with NaOH.

It was shown earlier that the somatic membrane of embryonic and early postnatal mammalian sensory neurons includes at least two types of calcium channels (Carbone & Lux, 1984; Fedulova, Kostyuk & Veselovsky, 1985; Nowycky, Fox & Tsien, 1985; Fox, Nowycky & Tsien, 1987*a,b*; Kostyuk, Shuba & Savchenko, 1988). The present work deals with the activity on cultured DRG neurons of mouse embryos. The membrane patches were depolarized from the holding potential level $V_h = -65$ mV (Kostyuk et al., 1988). Experiments were made on eight membrane patches containing one channel at 20–22°C. A conclusion about the presence of only one functional channel in each investigated patch was made on the basis of the complete absence of overlapping openings at all test potentials.

During single-channel experiments, the patch responses to 160-msec depolarizing pulses at a rate of 0.25–0.33 Hz were recorded after filtration (1 or 2 kHz bandwidth) in an analog form on a magnetic tape. After the experiment, the data were digitized at a frequency of 10 kHz and stored on computer hard disks. The channel openings and closings were detected as crossings of the line set at a half distance between zero current line and a level corresponding to the average open-channel amplitude. According to this, real current records were transformed into ideal form by setting all intermediate amplitudes to the level of zero current line or to the level of average open-channel amplitude. With half-amplitude threshold, the "dead time" t_d (maximal pulse duration in which current amplitude does not reach the threshold) equals 0.09 msec for frequency bandwidth $\Delta f = 2$ kHz and 0.18 msec for $\Delta f = 1$ kHz. In common case t_d is related to Δf as $t_d = 0.183/\Delta f$ (Colquhoun & Sigworth, 1983). The fitting of different time histograms to theoretical probability density functions (PDFs) for corresponding distributions was performed according to Brown et al. (1984). Because of insufficient analog and digital compensation of capacitative artifacts during data processing, we omitted the initial 1–2 msec from the beginning of real depolarization. This could not influence most of the measured histograms. However, upon determination of waiting-time histograms, the error could be significant. To minimize its possible effect, in each case the necessary shift corresponding to the duration of the initial distorted part of current event was introduced in the resulting histograms.

Results

After formation of a giga-seal between the pipette tip and the membrane surface of cultured mouse DRG neurons, unitary current pulses representing calcium inward fluxes could be observed in 60–70% of the investigated cells in response to depolarization of the membrane patch from holding potential level $V_h = -65$ mV (Fig. 1). The pulses appeared in test potential range $V_t = -15$ to +35 mV with a unitary amplitude of 0.6–0.3 pA that corresponds to the slope conductance of 7 ± 0.4 pS. At larger depolarizations, the current pulse amplitude decreased too much to be reliably resolved. The pulses tended to appear in bursts, as was already shown in previous measurements of calcium channel activity. We attribute the activity observed to the functioning of HTI calcium channels in DRG neurons of mouse embryos. The following arguments are in favor of this: (i) the observed activity appears in the potential range characteristic for this type of channel (Nowycky et al., 1985; Fox et al., 1987*a,b*; Kostyuk et al., 1988); (ii) activation of HTI channel is the most frequent with Ca^{2+} as a charge carrier (Kostyuk et al., 1988); (iii) after computer idealization of single-channel recordings and their subsequent averaging, the current wave forms obtained demonstrate prominent inactivation, which resembles macroscopic HTI currents recorded from the whole-cell membrane (*see* Fig. 1); (iv) we did not find any difference in unitary current amplitude at high depolarizations for different patches; conduc-

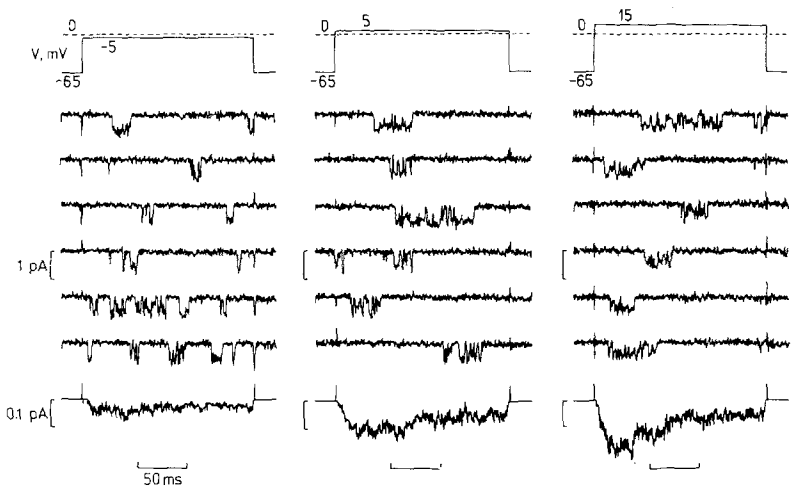

Fig. 1. Inward currents through a single high-threshold calcium channel in mouse sensory neuron membrane in response to 6 successive depolarizations for each potential. The records were obtained in the cell-attached configuration with 60 mM Ca as a charge carrier in the pipette. Lower traces: averages of 46, 52 and 64 idealized current records for test potentials −5, 5 and 15 mV.

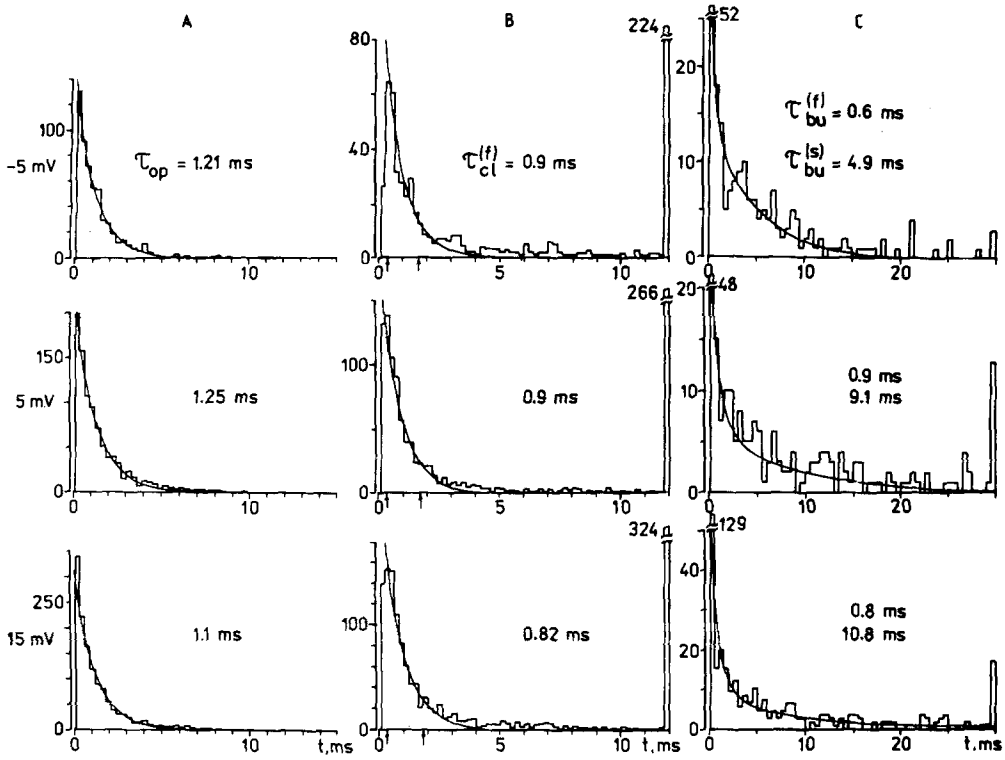

Fig. 2. Kinetic characteristics of single calcium channel functioning. (*A*) Open time, (*B*) closed time and (*C*) burst length histograms at three membrane potentials (indicated on the left) and their approximations by single (*A*,*B*) and biexponential (*C*) curves. *N* = number of events. Arrows in (*B*) indicate a part of the histogram used for approximation. The corresponding time constants are indicated near the histograms. Bin width for (*A*), (*B*) and (*C*) is 0.3, 0.2 and 0.5 msec, respectively. In this and subsequent figures, the last bin of the histograms contains all the rest of the events up to 100 msec. The figures near the last bin in (*B*) and first bin in (*C*) are equal to the quantity of events contained in these bins.

tance of the observed type of calcium channels is close to that of the HTI channel obtained on the same preparation if 60 mM Sr^{2+} was used as a charge carrier (Kostyuk et al., 1988); (v) distribution of open times for all test potentials and all investigated patches was monoexponential with a practically potential-independent time. constant, which is in agreement with previous observations for HTI channels (Kostyuk et al., 1988).

Figure 2 presents histograms for channel life times in different states and their approximations by single or double exponential functions using the

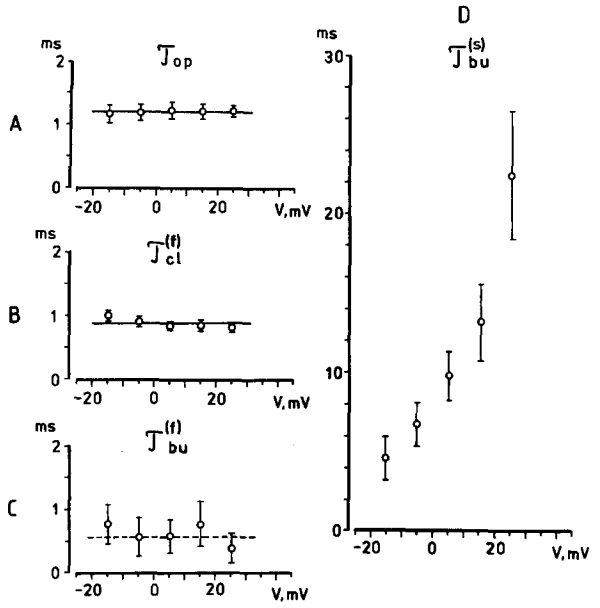

Fig. 3. Potential dependence of kinetic parameters of single calcium channel functioning. (*A*) Mean open time (τ_{op}), (*B*) mean time of intraburst gaps (τ_{cl}^{f}), (*C*) "fast" component of the burst length (τ_{bur}^{f}) and (*D*) "slow" component of the burst length (τ_{bur}^{s}). Solid lines in *A* and *B* indicate the corresponding mean value for all test potentials; dashed line in *C* indicates the result of calculation according to Eq. (A9).

least-squares method. The open-time histograms (Fig. 2*A*) were monoexponential for all test potentials with only slightly potential-dependent mean open time $\tau_{op} = 1.2$ msec (Fig. 3*A*). The closed-time histograms had a more complicated form (Fig. 2*B*). Most events fell on its initial part (0–2 msec) followed by a low-amplitude "tail" lasting up to 100 msec. Such distribution was observed at all test potentials. The "fast" component of this distribution could be successfully fitted by a single exponential function with time constant $\tau_{cl}^{f} = 0.9$ msec. As can be seen from Fig. 3*B*, the latter was practically independent of test potential.

The open-time histogram (Fig. 2*A*) and the "fast" component of the closed-time histogram (Fig. 2*B*) evidently represent potential-independent conformational transitions of the channel between closed, activated and open states (transitions $A \underset{b}{\overset{a}{\rightleftharpoons}} O$), which produce its "flickering" during bursts. These transitions do not involve charge movement, but only local transformations of the channel gating mechanism.

Small contribution of the "slow" tail to the overall closed-time histogram indicates a significantly higher number of gaps during the burst than that of interburst closed times. As such channel behavior was observed at all test potentials, we used a simple procedure for the identification of bursts by choosing a characteristic time interval, which would include all intraburst channel closures. Proceeding from the experimentally obtained closed-time histograms, this interval could be $O \leq t \leq 3\tau_{cl}^{f}$ (Magleby & Pallotta, 1983). All channel closures, which fell on this interval during identification of bursts, were considered as intraburst gaps and were neglected. Figure 2*B* presents histograms for burst durations obtained in such a way. They could be fitted by two exponentials—a "fast," practically potential-independent one with a time constant τ_{bur}^{f} of about 0.6 msec (Fig. 3*C*) and a "slow" one with a time constant τ_{bur}^{s} increasing from 4 msec at $V_t = -15$ mV to 20 msec at $V_t = 25$ mV (Fig. 3*D*). The "fast" component corresponds to short single openings of the channel not included in bursts, while the "slow" one reflects the distribution of real bursts. Physically the "fast" component represents the process of reaching an equilibrium between activated (*A*) and open (*O*) states of the channel, and the "slow" one the exponential decay of the total state $AO = A + O$. To understand a somewhat conflicting result $\tau_{bur}^{f} < \tau_{op}$, one can consider two boundary situations. In the first case, when $\tau_{op} \ll \tau_{cl}^{f}$ (or $\tau_{cl}^{f}/\tau_{op} \to \infty$) according to Eqs. (A7) and (A8) $\tau_{bur}^{f} \to \tau_{op}$, $\tau_{bur}^{s} \to 1/2\beta$ and $A_{bur}^{s} \to 2\beta\tau_{op}^{2}/\tau_{cl}^{f} \to 0$. Thus, most of events will be out of the bursts and the histogram of burst durations will approach the open-state histogram. In the second case, when $\tau_{op} \gg \tau_{cl}^{f}$ (or $\tau_{op}/\tau_{cl}^{f} \to \infty$), according to Eq. (A7) $\tau_{bur}^{f} \to \tau_{cl}^{f}$ and $\tau_{bur}^{s} \to \tau_{op}/2\beta\tau_{cl}^{f} \to \infty$. Experimentally, in the latter situation, practically all channel openings will be included in bursts and only those openings whose duration is less than τ_{cl}^{f} will be mostly out of bursts, contributing to the "fast" component of burst-length histogram. Thus, in general, it will always be $\tau_{bur}^{f} < \min\{\tau_{op}, \tau_{cl}^{f}\}$. Similar relations between time constants were observed by Brown et al. (1984).

The experimentally obtained values τ_{op}, τ_{cl}^{f} and τ_{bur}^{s} were used for determination of the constants b, a and β in the proposed model (Table 1). The corresponding expressions Eqs. (A5), (A9) and (A10) are given in the Appendix.

Table 1. Mean values of the constants a^{-1}, b^{-1}, α^{-1}, β^{-1}, τ_{cl}^{s} and τ_{cl}^{us} in msec for different potentials

V (mV)	a^{-1}	b^{-1}	α^{-1}	β^{-1}	τ_{cl}^{s}	τ_{cl}^{us}
−15	1.0	1.14	25.0	3.6	2.92	122.0
−5	0.9	1.16	14.0	5.6	2.74	35.7
5	0.82	1.24	11.3	8.2	2.6	22.0
15	0.86	1.22	6.6	11.1	2.27	9.6
25	0.82	1.24	5.4	18.9	2.17	6.7

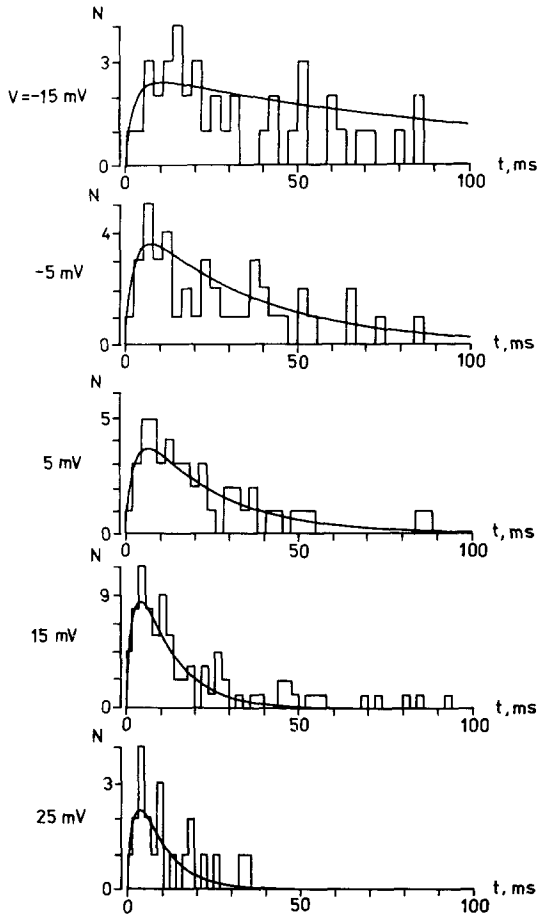

Fig. 4. Waiting-time histograms at different membrane potentials (indicated on the left) and their approximations by Eq. (A23). N = number of events. Bin width is 2.8, 2.8, 2.4, 2.0 and 1.8 msec for test potentials −15, −5, 5, 15 and 25 mV, respectively.

To identify α, the waiting-time histograms for the first channel opening were analyzed. These histograms, with sufficient accuracy, should be described in the proposed model by Eq. (A13) (*see* Appendix). As can be seen from Fig. 4, the waiting-time histograms had a maximum, which shifted to shorter time intervals with increasing depolarization. The amplitude and position of the maximum are very sensitive to the changes in α and β values in Eq. (A13). This makes this probability density function (PDF) very convenient for such identification. The approximation of the waiting-time histograms by Eq. (A13) is also presented in Fig. 4. The values for each test potential were determined using least square deviations between theoretical curves and experimental histograms, and the β values independently from the already known values of τ_{op}, τ^f_{cl} and τ^s_{bur} according to Eq. (A10). The obtained kinetic constants are summarized in Table 1.

Table 2. Comparison of experimental and theoretical values for relative contribution of "slow" and "very slow" potential-dependent components to the total closed-time distribution at different potentials

V (mV)	Theory		Experiment	
	A^s_{cl}	A^{vs}_{cl}	A^s_{itb}	A^{vs}_{itb}
−5	0.03	0.014	0.1	0.008
5	0.012	0.01	0.029	0.004
15	0.011	0.03	0.06	0.01

Thus, the complete set of rate constants determining the behavior of a single calcium channel was obtained in the frame of the model (Eq. (1)). To test the adequacy of such a description of the kinetic characteristics of the calcium channel, a comparison was made between the experimentally obtained closed-time distributions and theoretical ones calculated according to Eq. (A12). The relative amplitudes A^s_{cl} and A^{vs}_{cl} of the "slow" and "very slow" components of the closed-time histogram were defined by using Eq. (A14) with the experimental values of α, $\beta\tau^s_{cl}$ and τ^{vs}_{cl} (the latter two were determined from the waiting-time histograms). The time constant τ^f_{cl} and the amplitude of the "fast" component of the closed-time distribution inversely proportional to it (*see* Eq. (A12)) were determined by least square deviations between experimental and theoretical histograms. The results of this comparison are presented in Fig. 5*A*. The figure shows satisfactory agreement between the theoretical and experimental curves, thus supporting the possibility to use the proposed model for description of the kinetic behavior of single calcium channels. The values of τ^f_{cl} calculated for test potentials −5, 5 and 15 mV were 1.12, 0.98 and 1.00 msec, respectively, being close to those obtained from direct fitting of the "fast" component of the closed-time distribution by least squares fit procedure (*see* Fig. 2*B*), thus indicating that the error made during burst identification was not large.

Figure 5*B* presents the histograms of interburst time intervals and the results of their approximation by two exponents using least squares fit procedure. The values of τ^s_{itb} and τ^{vs}_{itb} (in msec) obtained for test potentials −5, 5 and 15 mV were as follows: 2.9 and 37.2, 2.5 and 22.5, and 2.2 and 12.8, respectively. They are very close to the time constants τ^s_{cl} and τ^{vs}_{cl} calculated independently from the waiting-time histograms (*see* Fig. 4 and Table 1).

Table 2 compares the values of amplitude ratios A^s_{cl} and A^{vs}_{cl} calculated from Eq. (A14), and the corresponding values A^s_{itb} and A^{vs}_{itb} obtained experimentally as the ratios of the amplitudes of two exponen-

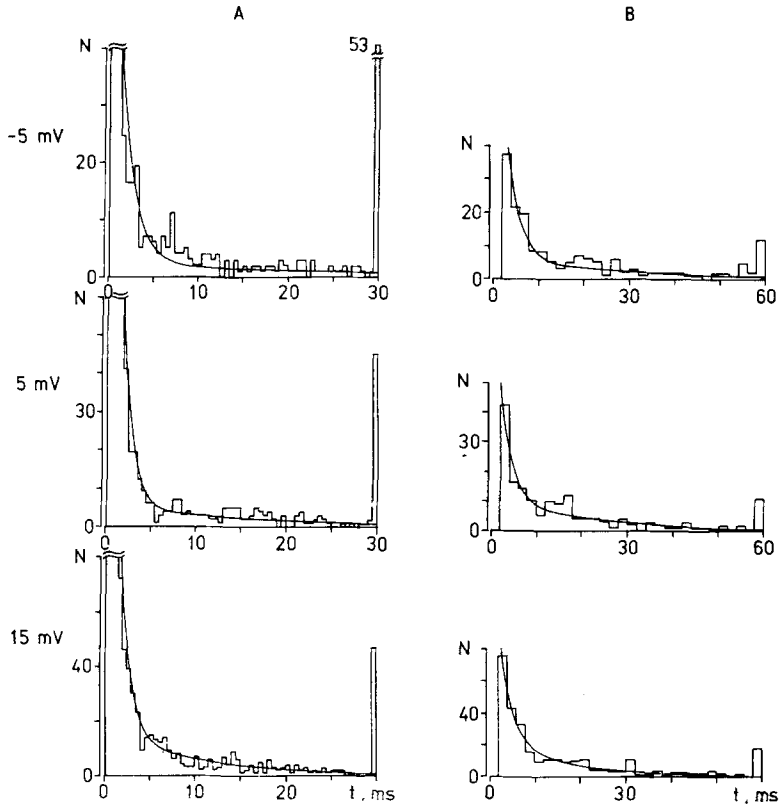

Fig. 5. (*A*) Closed time and (*B*) interburst shut time histograms at three membrane potentials (indicated on the left). N = number of events. (*A*) Bin width 0.5 msec, continuous lines = results of calculations according to Eq. (A22); (*B*) bin width 2 msec, continuous lines = results of biexponential fitting using least squares procedure. Corresponding time constants are in text.

tial components of the interburst closed times distribution (Fig. 5*B*) to the amplitude of the "fast" exponential component of total closed times distribution (Fig. 2*B*). The difference in bin size of the corresponding histograms was taken into account. It can be seen that the theory gives a two to four times lower value for the "slow" component (A_{cl}^{s} and two to three times higher value for the "very slow" component (A_{cl}^{vs}) as compared to experimental values A_{itb}^{s} and A_{itb}^{vs}. This discrepancy between theoretical and experimental evaluation of the relative contribution of different components to the overall closed-time histogram is not very large. It may be due to both inaccurate experimental measurements and to the approximate nature of Eqs. (A12)–(A15) compared with precise solutions of the system (A11).

The adequacy of the model (Eq. (1)) for other types of calcium channels was tested on LTI channels of neuroblastoma cells and HTN channels of PC-12 pheochromocytoma cells. The whole procedure of data fitting described above for HTI calcium channels of DRG neurons of mouse embryos was used. In general, this model was found to fit well to the data on LTI calcium channel activation. In comparison with HTI calcium channels, the only difference found are the potential dependence and the absolute values of mean channel open time. For LTI channels, it decreases from 0.8 to 0.3 msec as depolarization increases from −40 to 0 mV. Similar behavior of LTI calcium channel mean open time was observed for all divalent charge carriers. In contrast, permeant divalent ion species affected essentially the potential dependence of rate constants for the first two kinetic stages of the activation process that formally can be attributed to the transmembrane movement of gating particles.

A remarkable feature of activation kinetics for the HTN channel of PC-12 pheochromocytoma cells was the biexponential distribution of its open times. This indicates the presence of two open states for this channel with different life times. They were of the order of 0.5–0.2 msec and 1.8–2 msec for short and long lived states, respectively. A similar result was obtained for HTN calcium channels of bovine chromaffin cells (Hoshi & Smith, 1987). Indirect data in favor of the presence of two conducting states in the same preparation was obtained on the whole-cell level by Fenwick et al. (1982). The inadequacy of fitting open-time histograms of HTN calcium channels with single exponentials was also pointed out for DRG neurons of mouse embryos (Kostyuk et al., 1988). At the same time, our experiments on pheochromocytoma cells (Shuba &

Lyubanova, 1988) showed that the formalism of the model (Eq. (1)) describing the channel transition into activated state A through the Hodgkin-Huxley m^2 process can also be valid for HTN channels.

Discussion

Our analysis of the activity of HTI calcium channels in the membrane of mammalian sensory neurons confirms the possibility of an adequate description of the main experimental findings in the framework of a 4-state sequential kinetic model. This model has solved all difficulties that have arisen earlier during the analysis of a 3-state model. An important feature of the new model is the description of the closed-time histogram by the sum of three (not two) exponential components. The first "fast" component mainly reflects a potential-independent transition $A \overset{a}{\rightharpoonup} O$ with sufficient accuracy, while the two slower ones ("slow" and "very slow") reflect a potential-dependent transfer of charged gating particles. These three closed-time distribution components can be reliably detected in original current records, in which the "fast" one (mean time constant 0.9 msec) represents transient channel closing during a single burst of activity. Several bursts, in turn, aggregate into clusters with a mean intracluster closed time of about 3 msec. This "clustering" can be especially well observed at low depolarizations. Finally, closed intervals between clusters form the third "very slow" component of the total shut times distribution. Similar relations between different closed times were observed by Cavalie, Pelzer and Trautwein (1986) on single calcium channels in the membrane of isolated cardiomyocytes.

Drawing the conclusion about virtual potential independence of the last kinetic stage in the model (Eq. (1)), the limitations derived from the limited resolution of the recording system and the procedure of data processing should be taken into account. Using the data of Blatz and Magleby (1986), it is possible to show that in approximations (Eq. (A1)) and $t_d \ll \tau_{op}$, τ^f_{cl}, which are true for calcium channels and our recording conditions, real mean channel open time T_{op} and real mean intraburst shut time T^f_{cl} are related to measured times τ_{op} and τ^f_{cl} as follows $1/b = T_{op} \approx \tau_{op}(1 - t_d/\tau^f_{cl})$, $1/a = T^f_{cl} \approx \tau^f_{cl}(1 - t_d/\tau_{op})$. These expressions show that the consideration of t_d leads to a decrease of absolute values of mean channel open time by about 10% leaving it still potential independent, while T^f_{cl} will fall from 0.91 msec at −25 mV to 0.73 msec for +15 mV (data from Fig. 2). Thus, the conclusion about weak potential dependence of rate constants a and b for HTI channels seems to be correct.

As was already mentioned, contribution of the potential-dependent components to the overall closed-time distribution is negligible as compared with the "fast" potential-independent one (*see* Table 2); it does not change much with the changes in test potential. This conclusion fits well with the experimental data. In this respect, it should be noted that relations between the amplitudes of the potential-dependent and potential-independent components of the closed-time histogram observed by Hagiwara and Ohmori (1983) changed from 0.07 to 0.4 for a 25-mV depolarization; these conflicting results may be due to the presence in their experiments of several calcium channels in membrane patch.

Figure 5*A* shows that despite the theoretical probability density functions describe correctly the main amount of events in the closed-time histograms (~96%), still a small part of them (~4%) form an "extraslow" tail that cannot be described by Eq. (A12). Most probably, this tail is due to inactivation of a calcium channel. The presence of this process in the investigated test potential range can be shown by average current records as in Fig. 1; a definite decrease in the current amplitude can be seen after the latter reaches its maximum value. In our calculations, the identification of potential-dependent rate constants α and β was based on the histograms of burst duration and waiting times to the first channel opening. These histograms are least affected by the inactivation process. Due to this fact, we could avoid distortions of the results describing activation of the calcium channel by superposition of inactivation. An extention of the model to include inactivated channel states seems to be premature now because of insufficient experimental data about inactivation kinetics of single calcium channels.

The presented determination of the rate constants α and β responsible for the initial two stages of channel activation seems to be quite rigorous. Therefore, it would be desirable to evaluate the degree of their potential dependence. Figure 6 presents in a semilogarithmic scale the mean values of α and β at five different test potentials. They fall on straight lines having semilogarithmic slopes of about +1.1 and −1.1. Thus, the potential dependence of $\alpha(V)$ and $\beta(V)$ rate constants is, as expected, of an exponential type. The logarithm of the relation $\alpha(V)/\beta(V)$ has a slope of 2.2 representing the effective valency of a postulated single gating m-particle in case of its transmembrane transition during channel activation. Similar values (2.4–2.9) have been obtained in this analysis of the asymmetric displacement currents related to calcium channel activation in nerve cell membrane (Kostyuk et al., 1981).

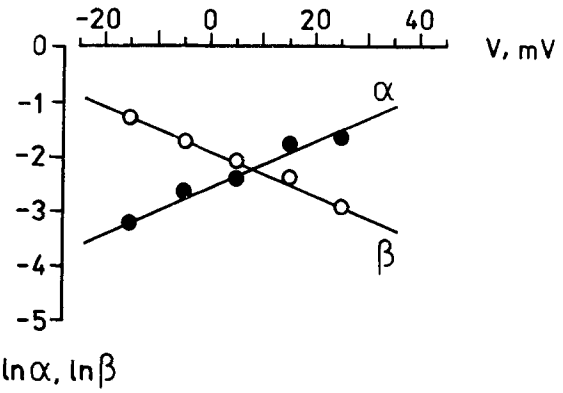

Fig. 6. Potential dependence of the rate constants α and β.

In conclusion, we may relate the calculated rate constants $\alpha(V)$ and $\beta(V)$ to the time constants $\tau_m(V)$ and $\tau_{tail}(V)$ of macroscopic current relaxation obtained during membrane depolarization (m-process) and repolarization ("tail"-process). At large depolarizations, the proposed model corresponds exactly to the modified Hodgkin-Huxley equations for calcium channel activation using the square power of the m-variable. Under these conditions $\beta(V) \ll \alpha(V) \ll a,b$ and the following relation holds $\alpha^{-1}(V) \approx \tau_m(V)$. Consequently, when the test potential is shifted to more positive values, the value of $\tau_m(V)$ must decrease exponentially from 6.7 msec at V_t = 15 mV to 2.8 msec at V_t = 35 mV (*see* Fig. 6). Similar voltage dependence of $\tau_m(V)$ was obtained by Kostyuk et al. (1981) during their study of the calcium current kinetics in the membrane of snail neurons. During repolarization, the time constant of the calcium tail current ($\tau_{tail}(V)$) must practically coincide with the life time of the single channel burst ($\tau^s_{bur}(V)$). At small repolarization potentials, when $\alpha(V) \ll \beta(V) \ll a,b$ the value of $\tau_{tail}(V) \approx (a + b)/2b\beta(V)$. Thus, during repolarization of the membrane to these potentials, τ_{tail} values must decrease exponentially (*see* Fig. 6); however, at very high negative potentials, when $\alpha(V) \ll a,b \ll \beta(V)$ this decrease should be limited and τ_{tail} should theoretically become equal to the mean open life time of the channel $\tau_{tail} \approx b^{-1}$. Qualitatively, such a voltage dependence of $\tau_{tail}(V)$ has been recently observed by Veselovsky et al. (1985). A more detailed quantitative analysis of the voltage dependence of $\tau_{tail}(V)$ is now in progress.

References

Amano, T., Richardson, E., Nirenberg, M. 1972. Neurotransmitter synthesis of neuroblastoma clones. *Proc. Natl. Acad. Sci. USA* **69**:258–263

Blatz, A.L., Magleby, K.L. 1986. Correcting single channel data for missed events. *Biophys. J.* **49**:967–980

Brown, A.M., Lux, H.D., Wilson, D.L. 1984. Activation and inactivation of single calcium channels in snail neurons. *J. Gen. Physiol.* **83**:751–769

Brown, A.M., Tsuda, Y., Wilson, D.L. 1983. A description of activation and conduction in calcium channels based on tail and turn-on current measurements in the snail. *J. Physiol. (London)* **344**:549–584

Byerly, L., Chase, P.B., Stimers, J.B. 1984. Calcium current activation kinetics in neurones of the snail *Lymnaea stagnalis*. *J. Physiol. (London)* **348**:187–207

Byerly, L., Hagiwara, S. 1982. Calcium currents in internally perfused nerve cell bodies of *Limnaea stagnalis*. *J. Physiol. (London)* **322**:503–528

Carbone, E., Lux, H.D. 1984. A low voltage-activated, fully inactivating Ca channel in vertebrate sensory neurons. *Nature (London)* **310**:501–503

Cavalie, A., Pelzer, D., Trautwein, W. 1986. Fast and slow gating behaviour of single calcium channels in cardiac cells. *Pfluegers Arch.* **406**:241–258

Colquhoun, D., Hawkes, A.G. 1981. On the stochastic properties of single ion channels. *Proc. R. Soc. London B* **211**:205–235

Colquhoun, D., Sigworth, F.J. 1983. Fitting and statistical analysis of single channel records. *In:* Single Channel Recording. B. Sakmann and E. Neher, editors. pp. 191–263. Plenum, New York

Fedulova, S.A., Kostyuk, P.G., Veselovsky, N.S. 1981. Calcium channels in the somatic membrane of the rat dorsal root ganglion neurons, effect of cAMP. *Brain Res.* **214**:210–214

Fedulova, S.A., Kostyuk, P.G., Veselovsky, N.S. 1985. Two types of calcium channels in the somatic membrane of newborn rat dorsal root ganglion neurons. *J. Physiol. (London)* **359**:431–446

Fenwick, E.M., Marty, A., Neher, E. 1982. Sodium and calcium channels in bovine chromaffin cells. *J. Physiol. (London)* **331**:599–635

Fox, A.P., Nowycky, M.C., Tsien, R.W. 1987*a*. Kinetic and pharmacological properties distinguishing three types of calcium currents in chick sensory neurones. *J. Physiol. (London)* **394**:149–172

Fox, A.P., Nowycky, M.C., Tsien, R.W. 1987*b*. Single-channel recordings of three types of calcium channels in chick sensory neurones. *J. Physiol. (London)* **394**:173–200

Green, L.A., Tischler, A.S. 1976. Establishment of a noradrenergic clonal line of a rat adrenal pheochromocytoma cells which respond to nerve growth factor. *Proc. Natl. Acad. Sci. USA* **73**:2424–2428

Hagiwara, S., Byerly, L. 1983. The calcium channel. *Trends Neurosci* **6**:189–193

Hagiwara, S., Ohmori, H. 1983. Studies of single calcium channel currents in rat clonal pituitary cells. *J. Physiol. (London)* **336**:649–661

Hamill, O.P., Marty, A., Neher, E., Sakmann, B., Sigworth, F.J. 1981. Improved patch-clamp techniques for high-resolution current recording from cells and cell-free membrane patches. *Pfluegers Arch.* **391**:85–100

Hoshi, T., Smith, S.J. 1987. Large depolarization induces long openings of voltage-dependent calcium channels in adrenal chromaffin cells. *J. Neurosci.* **7**:571–580

Kostyuk, P.G., Krishtal, O.A., Pidoplichko, V.I. 1981. Calcium inward current and related charge movements in the membrane of snail neurones. *J. Physiol. (London)* **310**:403–421

Kostyuk, P.G., Krishtal, O.A., Shakhovalov, Yu.A. 1977. Separation of sodium and calcium currents in the somatic membrane of mollusc neurones. *J. Physiol. (London)* **270**:545–568

Kostyuk, P.G., Shuba, Y.M., Savchenko, A.N. 1986. Single channels of low- and high-threshold calcium currents in the membrane of the mouse sensory neurones. *Neurophysiology (Kiev)* **18**:412–416

Kostyuk, P.G., Shuba, Ya.M., Savchenko, A.N. 1988. Three types of calcium channels in the membrane of mouse sensory neurons. *Pfluegers Arch.* **411**:661–669

Krishtal, O.A., Pidoplichko, V.I., Shakhovalov, Y.A. 1980. Properties of single calcium channels in the neuronal membrane. *Bioelectrochem. Bioenerg.* **7**:195–207

Magleby, K.L., Pallotta, B.S. 1983. Burst kinetics of single calcium-activated potassium channels in cultured rat muscle. *J. Physiol. (London)* **344**:605–624

Nowycky, M.C., Fox, A.P., Tsien, R.W. 1985. Three types of neuronal calcium channel with different calcium agonist sensitivity. *Nature (London)* **316**:440–443

Shuba, Ya.M., Lyubanova, O.P. 1988. Calcium permeability of PC-12 pheochromocytoma cells. *Biol. Membranes (Moscow)* **5**:698–710

Shuba, Ya.M., Savchenko, A.N. 1985. Single calcium channels in rat dorsal root ganglion neurons. *Neurophysiology (Kiev)* **17**:673–682

Skibo, G.G., Koval, L.M. 1984. Ultrastructural characteristics of synaptogenesis in monolayers cultures of spinal cord. *Neurophysiology (Kiev)* **16**:336–343

Tchuppina, L.M. 1981. Electrophysiological and neurochemical characteristics of neuroblasts of newborn rat cortex in cultured tissue. *Sechenov Physiol. Zhurn. SSSR* **67**:497–505

Veselovsky, N.S., Kostyuk, P.G., Fedulova, S.A., Shirokov, R.E. 1985. Deactivation of calcium currents in the somatic membrane of dorsal root ganglion neurons with removal of the membrane potential depolarization shift. *Neurophysiology (Kiev)* **17**:682–691

Received 29 November 1988; revised 3 March 1989

Appendix

Analysis of the Stochastic Properties of a 4-State Model for Calcium Channel Activation

The general approach to the analysis of such models has been formulated by Colquhoun and Hawkes (1981). In the present paper, we developed a clearer formalism to obtain probability density functions (PDFs) that will describe experimental distributions of the channel life times in different conductance states without using numerical methods. Characteristically, for calcium channel approximation

$$a,b \gg \alpha,\beta \tag{A1}$$

this formalism leads to simplified analytically tractable solutions, which can be directly used for independent identification of four different rate constants α, β, a and b introduced in the frame of the proposed model (Eq. (1)).

PDFs for Distributions of Burst Durations $P_{bur}(t)$ and Open Life Times $P_{op}(t)$

The approximation (Eq. (A1)) reflects the bursting nature of calcium channel activity based on channel transitions between states O and A. The problem of $P_{bur}(t)$ determination corresponds to the analysis of the evolution of probabilities of the channel $Q_O(t)$ and $Q_A(t)$ from the states O and A into the state C. It can be described by the system of two kinetic equations with the initial conditions $Q_O(O) = I$, $Q_A(O) = 0$ (Colquhoun & Hawkes, 1981).

Experimentally, the burst duration is usually measured as the interval between the beginning of the first current pulse in the burst and the end of the last one (so-called "apparent" duration, which differs from the "true" duration, *see* Colquhoun and Hawkes (1981)). Thus, $P_{bur}(t) = -d/dt\ Q_O(t)$ and after simple calculations we can find

$$P_{bur}(t) = [S_1(b - S_2)e^{-S_1 t} + S_2(S_1 - b)e^{-S_2 t}](S_1 S_2)^{-1} \tag{A2}$$

where

$$S_{\frac{1}{2}} = \tfrac{1}{2}\{a + b + 2\beta \pm [(a + b + 2\beta)^2 - 8b\beta]^{1/2}\} \tag{A3}$$

are the roots of the characteristic equation (Colquhoun & Hawkes, 1981).

To determine $P_{op}(t)$, it is necessary and sufficient to assume $a = 0$ in Eqs. (A2) and (A3). In this case, we obtain the usual expression of PDF for distribution of channel open life times

$$P_{op}(t) = \frac{1}{\tau_{op}} e^{-t/\tau_{op}} \tag{A4}$$

where

$$\tau_{op} = 1/b \tag{A5}$$

is the mean life time of the channel in the open state. The Eqs. (A4) and (A5) identify uniquely the rate constant b in the model (Eq. (1)).

For practical purposes, it is sufficient to transform the exact Eqs. (A2) and (A3) into an approximate form taking into account Eq. (A1). In this case, we obtain simplified expressions, which can be used for identification of the rate constants a and β:

$$P_{bur}(t) \approx \frac{1}{\tau_{op}} [e^{-t/\tau^f_{bur}} + A^s_{bur} e^{-t/\tau^s_{bur}}] \tag{A6}$$

where

$$\tau^f_{bur} = \left[\frac{1}{\tau_{op}} + \frac{1}{\tau^f_{cl}}\right]^{-1}, \quad \tau^s_{bur} = \tau_{op}[2\beta\tau^f_{bur}]^{-1} \tag{A7}$$

are the "fast" (f) and "slow" (s) characteristic times of the decay of channel bursting,

$$A^s_{bur} = 2\beta[\tau^f_{bur}]^2[\tau^f_{cl}]^{-1} \quad (A8)$$

is the ratio of the amplitudes of the "slow" and "fast" components,

$$\tau^f_{cl} = 1/a \quad (A9)$$

is the characteristic time for the process of "fast" return of the channel from the closed state into the open one and

$$1/\beta = 2\tau^s_{bur}\tau^f_{cl}[\tau_{op} + \tau^f_{cl}]^{-1} \quad (A10)$$

corresponds to the mean life time of the gating particle in an activated state.

PDFs for Distributions of Channel Life Times in Closed State $P_{cl}(t)$ and Waiting Times Until Its First Opening $P_{lat}(t)$

This problem corresponds to the analysis of the decay of the probabilities $Q_R(t)$, $Q_C(t)$ and $Q_A(t)$ of the channel being in closed states R, C and A into its open state O. Such decay can be described by the following system of equations

$$\begin{cases} \frac{d}{dt} Q_R(t) = \beta Q_c(t) - 2\alpha Q_R(t) \\ \frac{d}{dt} Q_c(t) = 2\alpha Q_R(t) + 2\beta Q_A(t) - (\alpha + \beta) Q_c(t) \\ \frac{d}{dt} Q_A(t) = \alpha Q_c(t) - (a + 2\beta) Q_A(t) \end{cases} \quad (A11)$$

with different initial conditions being $Q_A(O) = I$, $Q_C(O) = Q_R(O) = 0$, for definition of $P_{cl}(t) = -d/dt[Q_R(t) + Q_C(t) + Q_A(t)] = aQ_A(t)$ and $Q_R(O) = I$, $Q_C(O) = Q_A(O) = 0$ for the calculation of $P_{lat}(t) = aQ_A(t)$.

Strict analysis of the exact solution of the system (Eq. (A11)) is difficult. Fortunately, an approximation (Eq. (A1)) allows us to obtain the roots of the characteristic equation for the system Eq. (A11)) in an obvious form: $k_1 = 1/\tau^f_{cl} \approx a$ (*see* Eq. (A9)), $k_2 = 1/\tau^s_{cl} \approx \frac{1}{2}[3\alpha + \beta + (\alpha^2 + 6\alpha\beta + \beta^2)^{1/2}]$, $k_3 = 1/\tau^{vs}_{cl} \approx \frac{1}{2}[3\alpha + \beta - (\alpha^2 + 6\alpha\beta + \beta^2)^{1/2}]$. This leads to the following approximate expressions, which are sufficiently accurate to be used for independent identification of the rate constant a and α:

$$P_{cl}(t) = \frac{1}{\tau^f_{cl}}[e^{-t/\tau^f_{cl}} + A^s_{cl}e^{-t/\tau^s_{cl}} + A^{vs}_{cl}e^{-t/\tau^{vs}_{cl}}], \quad (A12)$$

$$P_{lat}(t) = (\tau^{vs}_{cl} - \tau^s_{cl})[e^{-t/\tau^{vs}_{cl}} - e^{-t/\tau^s_{cl}}] \quad (A13)$$

where we introduced

$$A^s_{cl} = \frac{2[\beta\tau^f_{cl}]^2\tau^{vs}_{cl}}{(\tau^{vs}_{cl} - \tau^s_{cl})(2\alpha\tau^{vs}_{cl} - 1)}, \quad A^{vs}_{cl} = \frac{2[\beta\tau^f_{cl}]^2\tau^s_{cl}}{(\tau^{vs}_{cl} - \tau^s_{cl})(1 - 2\alpha\tau^s_{cl})} \quad (A14)$$

the ratios of the amplitudes of the "slow" (s) and "very slow" (vs) components to the amplitude of the "fast" component in $P_{cl}(t)$ ($\tau^{vs}_{cl} > \tau^s_{cl} > \tau^f_{cl}$),

$$1/\alpha = (2\tau^s_{cl}\tau^{vs}_{cl})^{1/2} \quad (A15)$$

characterizes the mean life time of the gating particle in the resting state.

Comparison of the expressions for open time $P_{op}(t)$ (Eq. (A4)), burst length $P_{bur}(t)$ (Eq. (A6)), closed time $P_{cl}(t)$ (Eq. (A12)) and waiting time $P_{lat}(t)$ (Eq. (A13)) PDFs with the corresponding histograms obtained experimentally at different membrane potentials allows us to determine the time constants $\tau_{op}(V)$ (Eq. (A5)), $\tau^f_{cl}(V)$ (Eq. (A9)), $1/\alpha(V)$ (Eq. (A10)) and $1/\beta(V)$ (Eq. (A15)) and, thus to identify a complete set of rate constants introduced in the frame of simplified model (Eq. (1) and (A1)) for calcium channel activation.

In conclusion, it should be mentioned that the PDFs $P_{bur}(t)$, $P_{cl}(t)$ and $P_{lat}(t)$ for the channel with three closed states differ substantially from those of a channel model with two closed states. For example, the closed time PDF $P_{cl}(t)$ for the model (Eq. (1)) is described by the sum of three exponentials in contrast to two exponentials for the three-state sequential model (Fenwick et al., 1982; Hagiwara & Ohmori, 1983; Brown et al., 1984); the PDF $P_{lat}(t)$ in the approximation (Eq. (A1)) contains the difference between "very slow" and "slow" exponents as was expected from the modified Hodgkin-Huxley model, but not the difference between "slow" and "fast" ones as in the model analyzed by Brown et al. (1984); the amplitude of the "fast" component in the burst length PDF $P_{bur}(t)$ exceeds largely the amplitude of the "slow" component, whereas Hagiwara and Ohmori (1983) and Brown et al., (1984) present expressions in which both amplitudes are close to each other. These differences can be used for critical evaluation of different simplified models of calcium channel activation as well as for choosing the approximate model for the analysis of gating mechanisms of other ion channels with bursting activity.